SO₂ enhances aerosol formation from anthropogenic volatile organic compound ozonolysis by producing sulfur-containing compounds

Zhaomin Yang[1], Kun Li[1], Narcisse Tchinda Tsona[1], Xin Luo[2], Lin Du[1]

[1]Environment Research Institute, Shandong University, Qingdao, 266237, China

[2]Technology Center of Qingdao Customs, Qingdao, 266003, China

Correspondence to: Lin Du (lindu@sdu.edu.cn)

Abstract. Sulfur dioxide (SO_2) can affect aerosol formation in the atmosphere, but the underlying mechanisms remain unclear. Here, we investigate aerosol formation and composition from the ozonolysis of cyclooctene with and without SO_2 addition in a smog chamber. Liquid chromatography equipped with high-resolution tandem mass spectrometry measurements indicate that monomer carboxylic acids and corresponding dimers with acid anhydride and aldol structures are important components in particles formed in the absence of SO_2. A 9.4–12.6 time increase in particle maximum number concentration is observed in the presence of 14–192 ppb SO_2. This increase is largely attributed to sulfuric acid (H_2SO_4) formation from the reactions of stabilized Criegee intermediates with SO_2. In addition, a number of organosulfates (OSs) are detected in the presence of SO_2, which are likely products formed from the heterogeneous reactions of oxygenated species with H_2SO_4. The molecular structures of OSs are also identified based on tandem mass spectrometry analysis. It should be noted that some of these OSs have been found in previous field studies but were classified as compounds from unknown sources or of unknown structures. The observed OSs are less volatile than their precursors and therefore are more effective contributors to particle formation and growth, partially leading to the increase in particle volume concentration under SO_2-presence conditions. Our results provide an in-depth molecular-level insight into how SO_2 alters particle formation and composition.

1 Introduction

Secondary organic aerosol (SOA) accounts for a large fraction of the organic aerosol mass. The atmospheric oxidation of anthropogenic volatile organic compounds (AVOCs) can produce low-volatility organic products that contribute to SOA formation and growth (Kelly et al., 2018; Fan et al., 2020). The oxidation of AVOCs can dominate SOA formation under severe haze episodes (Nie et al., 2022; He et al., 2020; Huang et al., 2019; Qiu et al., 2020). Thus, AVOCs have been commonly considered as significant SOA precursors. SOA can negatively impact air quality, global climate, and public health (Nault et al., 2021; Zhu et al., 2017). To better understand air pollution and develop effective particle control strategies, it is necessary to investigate the formation mechanism and molecular composition of anthropogenic SOA.

Recently, the impacts of inorganic gases on aerosol chemistry have received significant attention (Deng et al., 2022). In particular, there is increasingly much evidence that sulfur dioxide (SO_2) can modulate SOA formation and composition (Ye et al., 2018; Stangl et al., 2019; Liu et al., 2017). Liu et al. (2017) reported that SOA formation from cyclohexene photooxidation was inhibited by atmospherically relevant concentrations of SO_2, as a result of the reaction of hydroxyl radical ($\cdot OH$) with SO_2 (to form sulfuric acid (H_2SO_4)) competing with the $\cdot OH$ reaction with cyclohexene. They demonstrated that H_2SO_4-catalyzed SOA enhancement was not sufficient to compensate for the loss of $\cdot OH$ reactivity towards cyclohexene, leading to the suppression in cyclohexene SOA formation. On the other hand, SO_2 can enhance SOA formation and alter SOA composition by interacting with organic peroxides or stabilized Criegee intermediate (sCI) during the ozonolysis of alkenes (Stangl et al., 2019; Ye et al., 2018). For instance, under humid condition, the reactive uptake of SO_2 onto organic aerosols was obvious and reactions of SO_2 with organic peroxides could contribute to organosulfate (OS) formation (Wang et al., 2021a; Ye et al., 2018). H_2SO_4 originated from sCI-induced oxidation of SO_2 is also linked to OS production (Stangl

55   et al., 2019). OSs have been detected in different SO_2-alkene interaction areas (Hettiyadura et al., 2019; Wang et al., 2018; Bruggemann et al., 2020). Ubiquitous OSs may be used as tracers of SOA influenced by SO_2 emissions (Bruggemann et al., 2020). To further gain mechanistic insights into the complex roles of SO_2 in SOA formation, it is important to explore the chemical nature and formation mechanism of OSs.

60   Cycloalkenes emitted from diesel vehicles and industrial processes are a crucial class of AVOCs in the atmosphere. They can be used to explore key chemical processes involved in atmospheric oxidation and SOA formation (Räty et al., 2021). However, SOA formation chemistry from cycloalkenes has received less attention than that from linear or branched alkenes, leading to significant uncertainties in our understanding of

65   SOA. Recent studies have reported that ozonolysis of cycloalkenes could form highly oxidized products and have considerable SOA yield (Räty et al., 2021; Rissanen, 2018). Among the most common cycloalkenes (with 5 to 8 carbon atoms), cyclooctene has the largest potential to SOA formation (Keywood et al., 2004). Ozonolysis is the dominant oxidation pathway of cyclooctene with a reaction rate constant of 4.51×10^{-16} cm^3

70    $molecule^{-1}$ s^{-1} (298 K). Urban atmosphere is highly complex and may contain various concentrations of cycloalkenes and SO_2, which complicates SOA formation and composition. While most previous studies have identified compounds containing carbon, hydrogen, and oxygen atoms (CHO compounds) as important contributors to cycloalkene SOA (Hamilton et al., 2006; Gao et al., 2004; Räty et al., 2021), the

75   potential of OS formation from the ozonolysis of cyclooctene in the presence of SO_2 and the chemical processes behind OS formation remain unclear.

Given the significance of cycloalkene and SO_2 emissions in aerosol formation, we investigated the SO_2 effects on the formation and chemical composition of cyclooctene SOA. Aerosol particles were formed from the ozonolysis of cyclooctene in the absence

80   and presence of SO_2 in a smog chamber. Structural identifications of the observed products were reported and corresponding formation mechanisms were proposed. We report the mechanism showing how SO_2 impacts particle formation and growth based

on the observation of sulfuring-containing compounds. Our results provide a more comprehensively mechanistic understanding of the roles of SO_2 in modulating SOA

85   formation and composition.

2 Experimental methods

2.1 Particle production

Particle formation from the ozonolysis of cyclooctene ($k_{298 \text{ K}} = 4.51 \times 10^{-16}$ cm^3 $molecule^{-1}$ s^{-1}) was carried out under dark conditions in a 1.2 m^3 Teflon chamber

90   housed in a temperature-controlled room. A summary of experimental conditions and results is listed in Table 1. Detailed experimental equipment and methods have been described in our previous studies (Yang et al., 2022; Yang et al., 2021). Particle formation experiments were operated in a batch mode. Briefly, cyclooctene was introduced into the chamber by passing zero air through a tube containing a known

95   volume of cyclooctene (95%, Alfa). Then, cyclohexane (99.5%, Aladdin) was injected in excess (~130 ppm) into the chamber so that more than 98% of OH generated during the ozonolysis of cyclooctene were scavenged. Control experiments showed that the presence of cyclohexane could lead to the significant decrease in particle volume concentration (Fig. S1). When desired, SO_2 was added to the chamber from a SO_2

100   calibration cylinder. Initial concentration ratios of SO_2 to cyclooctene were in the range of ~0.07–1 ppb ppb^{-1} to simulate different polluted atmospheric conditions. The reactor was stabilized for 20 min under dark conditions to allow for mixing of species. Finally, ozonolysis of cyclooctene was initiated by introducing O_3 produced via a commercial ozone generator (WH-H-Y5Y, Wohuan, China). All experiments were performed at

105   room temperature (~295 K) and atmospheric pressure (~1 atm) without seed particles. Temperature and relative humidity (RH) inside the chamber were measured with a hygrometer (Model 645, Testo AG, Germany). O_3 and SO_2 concentrations over the course of ozonolysis were monitored by a Thermo Scientific model 49i O_3 analyzer and a Thermo Scientific model 43i-TLE SO_2 analyzer, respectively. The detection limits of

O$_3$ analyzer and SO$_2$ analyzer were 0.5 ppb and 0.05 ppb, respectively. Size distributions and volume concentrations of particles were continuously recorded using a scanning mobility particle sizer (SMPS), which consisted of differential mobility analyzer (Model 3082, TSI, USA) and ultrafine condensation particle counter (Model 3776, TSI, USA). The particle volume concentration was measured continuously until we observed a decrease. The particle formation experiments proceeded for 300 min before the collection of aerosol particles.

Table 1. Experimental conditions and results for particle formation experiments.

[Cyclooctene]$_0$ (ppb)	[O$_3$]$_0$ (ppb)	T (K)	RH (%)	SO$_2$ (ppb)	$\triangle$SO$_2$ [a] (ppb)	V_{H2SO4} [b] (μm^3 cm^{-3})	N_{max} [c] ×10^6 (cm^{-3})	$V_{particle}$ [d] (μm^3 cm^{-3})
195	839	296	25	-	-	-	0.14	151 ± 2.9
195	770	294	24	14	3.7	9.4	1.31	170 ± 5.7
195	800	294	22	28	8.9	22.6	1.05	191 ± 5.5
195	792	293	21	50	9.6	24.5	1.06	228 ± 4.2
195	730	292	20	100	9.5	24.3	1.54	264 ± 7.4
195	790	293	23	154	17.2	43.8	1.28	270 ± 5.0
191	743	295	24	192	14.2	35.9	1.77	280 ± 8.2

[a] $\triangle$SO$_2$ represents the consumed SO$_2$ concentration during the ozonolysis of cyclooctene.

[b] The volume concentration of particle-phase H$_2$SO$_4$ assuming a full conversion of SO$_2$ to H$_2$SO$_4$ with a density of 1.58 g cm^{-3} under moderate humidity conditions (Wyche et al., 2009; Ye et al., 2018).

[c] N_{max} denotes the maximum number concentration of aerosol particles during the ozonolysis of cyclooctene.

[d] $V_{particle}$ is the volume concentration of aerosol particles, which has been corrected for wall loss of particles. Errors represent standard deviation for particle formation experiments.

2.2 Particle collection and chemical characterization

Aerosol particles were collected on aluminum foils using a 14-stage low-pressure impactor (DLPI+, Dekati Ltd, Finland). All samples were stored in -20 ℃ freezer until analysis. Offline functional group measurements of aerosol particles were performed using an attenuated total reflectance-Fourier transform infrared spectrometer (ATR-FTIR, Vertex 70, Bruker, Germany). Before each measurement, the diamond crystal was thoroughly cleaned with ethanol and ultrapure water to eliminate the interference of ambient contaminants on functional group measurements of aerosol particles. ATR-FTIR spectra of blank aluminum foils and aerosol samples were recorded in the range of 4000–600 cm^{-1} at a resolution of 4 cm^{-1} with 64 scans. The data of ATR-FTIR spectra were recorded with the OPUS software.

Aerosol particles were also collected on polytetrafluoroethylene (PTFE) filters (0.22 μm pore size, 47 mm dimeter, TJMF50, Jinteng, China). The whole sample filters were extracted twice into 5 mL of methanol (Optima® LC-MS grade, Fisher Scientific) by ice sonication (KQ5200E, Kunshan Ultrasonic Instruments, China) for 20 min. Extracts were then filtered, concentrated to near dryness and subsequently reconstituted in 200 μL of 50:50 (v/v) methanol and ultrapure water. Blank filters were also subjected to the same extraction and preparation procedure. Obtained extracts of blank and sample filters were analyzed using a Thermo Scientific ultrahigh-performance liquid chromatograph, which was coupled with a high-resolution Q Exactive Focus Hybrid Quadrupole-Orbitrap mass spectrometer equipped with an electrospray ionization (ESI) source (UHPLC/ESI-HRMS). Samples were first separated on an Atlantis T3 C18 column (100 Å pores, 3 μm particle size, 2.1 mm × 150 mm, Waters, USA) at 35 ℃. The used binary mobile phase system consisted of ultrapure water with 0.1% (v/v) formic acid (A) and methanol with 0.1% (v/v) formic acid (B). The LC gradient employed was as follows: 0–3 min at 3% B, 3–25 min increased linearly to 50% B, 25–43 min ramped linearly to 90% B, 43−48 min returned to 3% B, and 48−60 min B held constant at 3% to re-equilibrate the column. The injected volume of samples and flow

rate were 2 µL and 200 µL min^{-1}, respectively. The ESI source was operated in both positive (+) and negative (−) ion modes to ionize analyte components with a scan range of mass-to-charge (*m/z*) 50 to 750. LC/ESI-MS parameter settings were as follows: 3.5 kV spray voltage (+), −3.0 kV spray voltage (−), 50 V S-lens radio frequency (RF) level (+), 50 V S-lens RF level (−), 320 °C capillary temperature, 2.76 × 10^5 Pa sheath gas (nitrogen) pressure, and 3.33 L min^{-1} auxiliary gas (nitrogen) flow. Data-dependent tandem mass spectrometry (MS/MS) analysis were also carried out by high-energy collision-induced dissociation (CID) with stepped collision energies of 20, 40, and 60 eV. For MS/MS experiments, an isolation width of 2 *m/z* units was applied. Other parameters were also selected in MS/MS experiments as follows: 2 × 10^5 automatic gain control (AGC) target, 50 ms maximum IT, 3 loop count, 1 × 10^5 minimum AGC target, 2–6 s apex trigger, and 6 s dynamic exclusion. The mass resolution of MS and MS/MS were 70000 (full width at half maximum, FWHM, at *m/z* 200) and 17500, respectively. Detailed data processes are reported elsewhere (Yang et al., 2021; Yang et al., 2022).

The double bond equivalent (DBE) value is the combined number of rings and double bonds in the product $C_cH_hO_oN_nS_s$ and could be calculated according to eq. 1. For organosulfate, the two S=O bonds in sulfate group were not considered based on calculations in previous studies (Wang et al., 2016; Riva et al., 2016b; Kuang et al., 2016). The DBE value of organosulfate reflects the unsaturation degree of its side carbon chain.

$$DBE = 1 + c + \frac{n - h}{2} \tag{1}$$

Kendrick mass defect (KMD) analysis could provide chemical insights into chemical compositions of complex organic mixtures (Kundu et al., 2017; Kenseth et al., 2020). The KMD value is same for homologous species that differ from each other only by their base units. CH$_2$ and the oxygen atom (O) are usually chosen as base units for Kendrick analysis of complex organic mass spectra. Kendrick mass (KM) could be converted into a new mass scale from the IUPAC mass (eq. 2 and 4). KMD is

determined as the difference between the nominal mass of a compound (the rounded integer mass) and KM (eq. 3 and 5).

$$KM_{CH_2} = m/z \times \frac{14.00000}{14.01565} \qquad (2)$$

$$KMD_{CH_2} = \text{Nominal mass} - KM_{CH_2} \qquad (3)$$

$$KM_O = m/z \times \frac{16.00000}{15.99492} \qquad (4)$$

$$KMD_O = \text{Nominal mass} - KM_O \qquad (5)$$

The saturation mass concentration (C^o, $\mu g\ m^{-3}$) of product i was also calculated based on its elemental composition using the following expression (Li et al., 2016):

$$\log_{10} C_i^o = (n_C^0 - n_C^i)b_C - n_O^i b_O - 2\frac{n_C^i n_O^i}{n_C^i + n_O^i}b_{CO} - n_N^i b_N - n_S^i b_S \qquad (6)$$

where n_C^0 is the reference carbon number; n_C^i, n_O^i, n_N^i, and n_S^i represent the numbers of carbon, oxygen, nitrogen, and sulfur atoms, respectively; b_C, b_O, b_N, and b_S denote the contribution of each carbon, oxygen, nitrogen, and sulfur atom to $\log_{10} C_i^o$; and b_{CO} is the carbon–oxygen nonideality.

2.3 Wall loss corrections

The wall loss rates of O_3 and SO_2 inside the chamber were determined to be 2.05×10^{-4} min^{-1} and 2.02×10^{-4} min^{-1} (Fig. S2), respectively, indicating that the losses of these two gas-phase species to the chamber walls were negligible over the course of experiments. The wall loss of cyclooctene (5.23×10^{-6} min^{-1}) was also negligible while its oxidation products may deposit to the inner walls. However, wall losses of gas-phase products could be mitigated due to excess O_3 concentration (Sect. S1). The quick oxidation and nucleation could provide attractive condensation surfaces for oxidation products, thereby reducing the product wall losses to some extent (Stirnweis et al., 2017). Although wall losses of organic vapors may underestimate the particle mass, this work mainly focuses on the characterization of particle composition rather than the absolute SOA yield.

Independent wall-loss experiments of ammonium sulfate ((NH_4)$_2SO_4$) particles

were also performed to determine the size-dependent wall-loss rate constants of particles inside the chamber. An aqueous $(NH_4)_2SO_4$ solution was added to a TSI Model 3076 atomizer to produce droplets. The droplets were passed through a silica gel diffusion dryer to get dry $(NH_4)_2SO_4$ particles and then were injected into the chamber. The size distributions of $(NH_4)_2SO_4$ particles were characterized using the SMPS for 6 h. The relationship between the wall-loss rate (k, h^{-1}) of particles and their size (d_p, nm) can be expressed as $k(d_p) = 1.20 \times 10^{-7} \times d_p^{2.32} + 20.59 \times d_p^{-1.39}$ based on size-dependent particle wall-loss correction method.

3 Results and discussion

3.1 SO$_2$ effects on aerosol formation

Insights into SO$_2$ effects on particle formation could be gained through investigating the number and volume concentration as well as size distribution of particles under various SO$_2$ level conditions. In the absence of SO$_2$, the particle number concentration increased burst within the first 20 min of cyclooctene ozonolysis and then decreased because of their coagulation and wall depositions, while the particle volume concentration increased gradually and reached its maximum within 240 min (Fig. S3). Elevating SO$_2$ level can result in significant increases in the number and volume concentration of particles (Fig. 1a), which is consistent with observations from previous studies (Ye et al., 2018; Yang et al., 2021). We observed a 9.4–12.6 time increase in particle maximum number concentration in the presence of 14–192 ppb SO$_2$ (Table 1). The promoted effect of SO$_2$ is shown more clearly in Fig. 1b, where SO$_2$ was seen to be consumed on similar timescale as particle formation. Specifically, upon initiation of cyclooctene ozonolysis, SO$_2$ concentration decreased and the particle volume concentration increased simultaneously. After cyclooctene was completely consumed, both SO$_2$ consumption and particle production slowed down. SO$_2$ consumption and particle formation resumed when more cyclooctene was introduced into the reactor. This result indicates that SO$_2$ may react with certain highly reactive species produced

from cyclooctene ozonolysis. For instance, reactions of SO_2 with sCI could form H_2SO_4

(Boy et al., 2013), which is a key specie for new particle formation (Lehtipalo et al.,

2018; Yao et al., 2018). Inorganic sulfate absorption at 617 cm^{-1} was observed in the

ATR-FTIR spectra of particles formed in cyclooctene/O_3/SO_2 systems (Fig. 2)

(Hawkins et al., 2010; Coury and Dillner, 2008), indicating the formation of H_2SO_4. We

assumed that all consumed SO_2 was converted to particle-phase H_2SO_4, which

represents an upper limit of the H_2SO_4 formation (Wyche et al., 2009; Ye et al., 2018).

The amount of H_2SO_4 produced could not fully account for the enhancement of particle

volume concentration (Table 1). H_2SO_4 has been considered as an important driver of

particle acidity (Tilgner et al., 2021). Acid catalysis induced by H_2SO_4 may also

promote the formation of additional organic products, leading to the increase in particle

volume concentration (Deng et al., 2021).

SO_2 can also affect the growth of new aerosol particles (Fig. 1c). Once O_3 was

introduced into the reactor, aerosol particles were produced rapidly. After cyclooctene

was depleted, the aerosol particle mass increased slowly. The initial stage of particle

formation was then defined as the time from reaction initiation to the complete

consumption of cyclooctene (~10 min). From Fig. 1c, in the initial stage of ozonolysis

(10 min), particles formed in cyclooctene/O_3/SO_2 systems had a smaller size mode than

those formed in cyclooctene/O_3 system, which may be attributed to the following two

factors. First, oligomers formed from sCI reactions with organic species could partition

into the condensed phase to contribute to particle growth (Riva et al., 2017). SO_2

presence may lead to the decrease in these oligomers because SO_2 can compete with

organic species to react with sCI. Second, counterbalancing the reduction of oligomers

via sCI + SO_2 reactions is the production of H_2SO_4. The production of more new

particles in cyclooctene/O_3/SO_2 systems could provide more condensation sinks.

Organic vapors that can condense onto particles are dispersed via new particles,

resulting in small particle size at the initial phase of cyclooctene/O_3/SO_2 systems

(Stangl et al., 2019). Interestingly, particles could grow quickly in the presence of SO_2.

At 300 min reaction time, particles formed in the presence of SO_2 even had slightly larger sizes than those formed in the absence of SO_2. H_2SO_4-catalyzed heterogenous

260   reactions could produce lower-volatile organic species from higher-volatile reactants in the aerosol phase (Yang et al., 2020; Han et al., 2016). Semi-volatile species could undergo evaporation after partitioning to the aerosol phase while low-volatile products generally have a negligible evaporation rate from the aerosol phase. Low-volatile products formed via H_2SO_4-catalyzed heterogenous reactions could build particle mass

265   at a rate almost equal to the condensation rate and thus effectively facilitate the particle growth in cyclooctene/O_3/SO_2 systems (Apsokardu and Johnston, 2018).
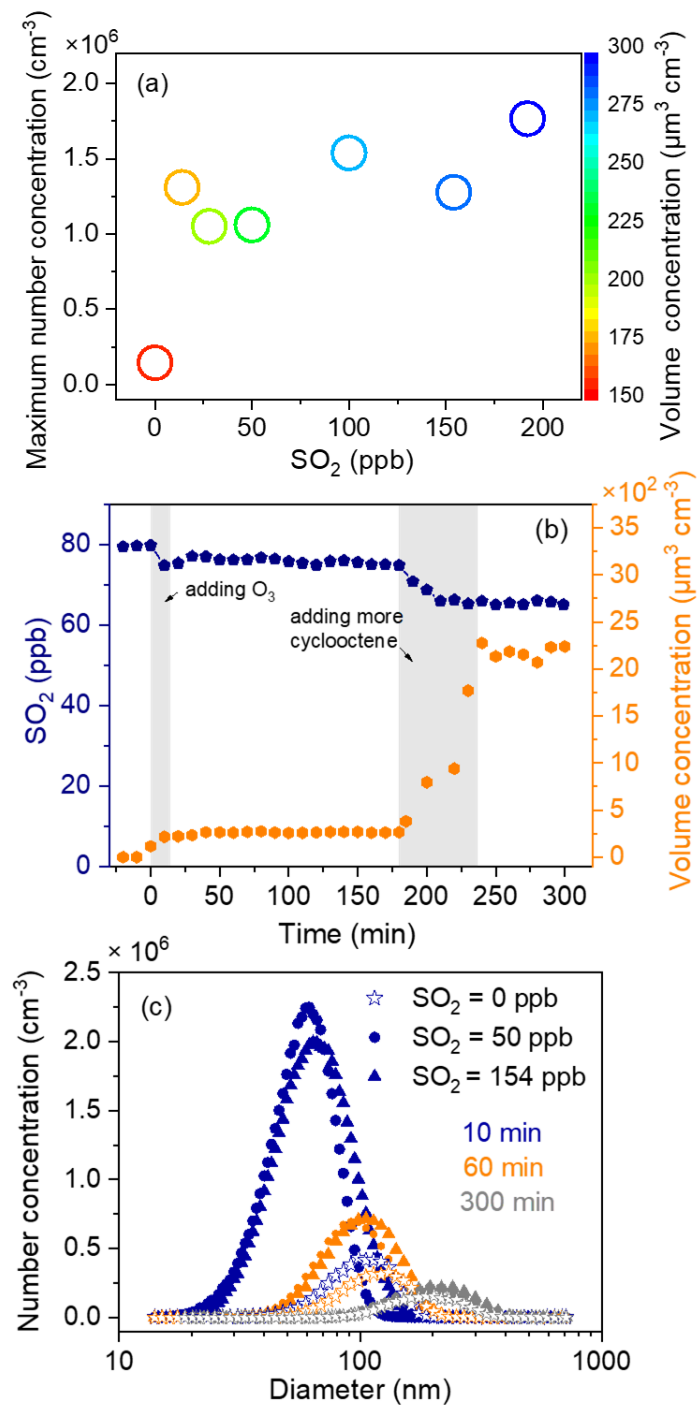
Figure 1. Particle formation from the ozonolysis of cyclooctene under various SO_2 conditions. (a) Maximum particle number concentration as a function of initial SO_2 level. Circle color represents particle volume concentration. (b) Temporal profiles of SO_2 concentration and particle volume concentration. (c) Size distributions of aerosol particles formed with various SO_2 concentrations at 10, 60, and 300 min after the after the initiation of cyclooctene ozonolysis.
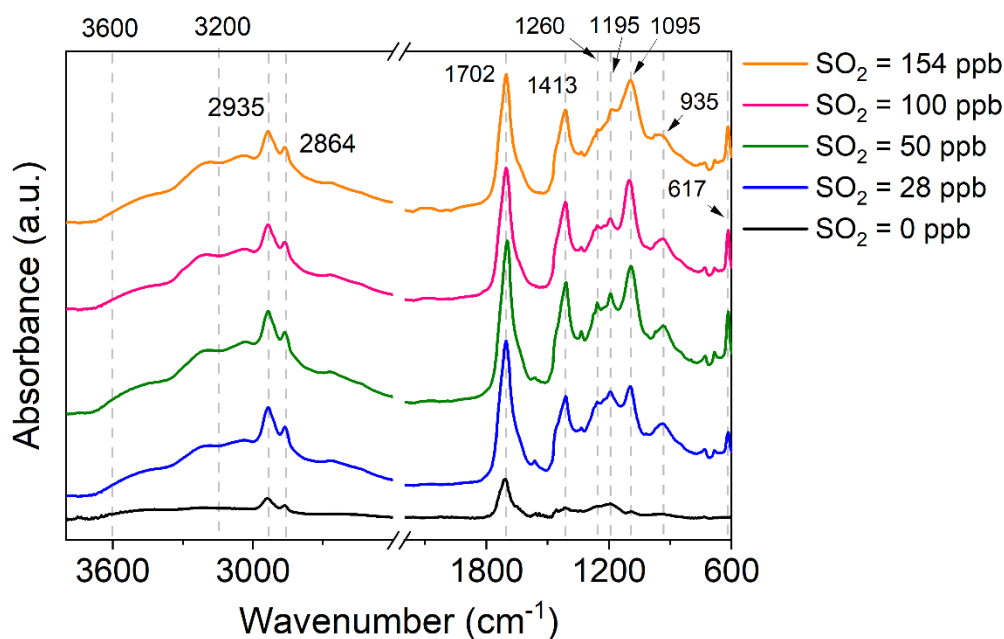
Figure 2. ATR-FTIR spectra of aerosol particles generated from cyclooctene ozonolysis in the presence of different SO_2 concentration.

3.2 Aerosol chemical composition under SO_2-free condition

Figure 3 shows the base peak chromatograms (BPCs) of cyclooctene-derived particles in the absence of SO_2. The chromatograms of blank filter showed clearly no peaks eluted at retention times (RTs) between 0 and 30 min while there were several significant peaks for cyclooctene SOA chromatograms in both positive and negative ion modes. Each chromatogram peak of cyclooctene SOA represents at least one ion, and major peaks are only labeled with the mass of the most abundant single ion. Compared to the negative chromatogram of cyclooctene SOA, the corresponding label ions in the positive chromatogram were 24 Da higher in mass. This is consistent with the fact that many ions produce adducts with sodium ion ($[M + Na]^+$) in positive ion mode, while negative ion mode leads to the production of deprotonated ions ($[M – H]^-$) (Mackenzie-Rae et al., 2018). From Fig. 3, products with molecular weight (MW) < 200 Da eluted from the column at shorter RT than those with MW > 200 Da. Low-molecular-weight products (MW < 200 Da) likely correspond to small monomer type compounds (hereafter termed as monomeric products), which are directly originated

from the ozonolysis of cyclooctene. Compounds with MW > 200 Da mainly dominate the later part of the chromatogram, and they may be homo or heterodimeric species (hereafter noted as dimeric products) formed using two monomeric products as building

295   blocks.
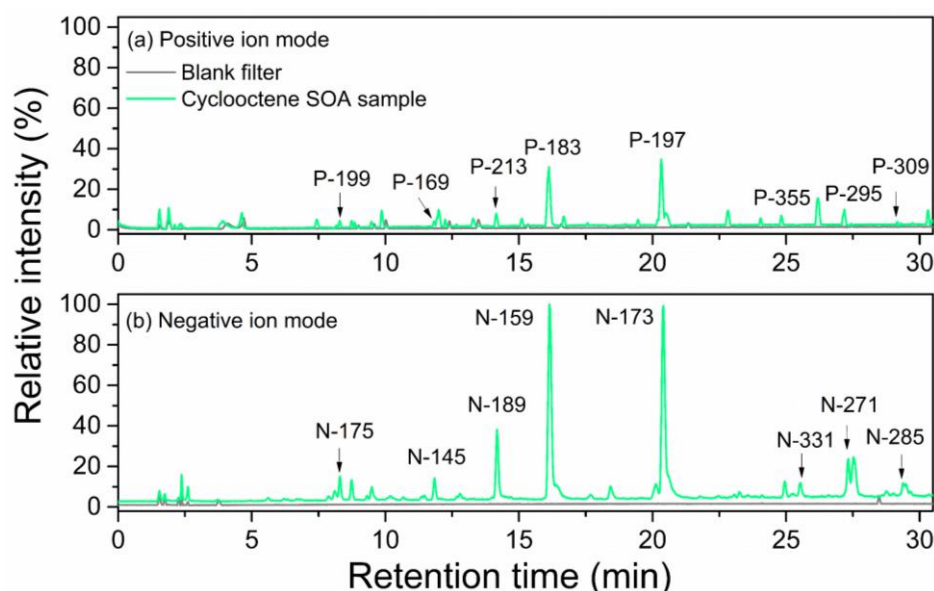
Figure 3. Base peak chromatograms of both blank filter and particles generated from the ozonolysis of cyclooctene in the absence of SO_2. Labels represent the most abundant

300   single ion of each peak. (a) Positive ion mode. (b) Negative ion mode.

Possible structures of major monomeric products were proposed based on their accurate *m/z*, fragmentation mass spectra, and previous mechanistic insights. Note that the fragmentation of $[M + Na]^+$ is relatively difficult (Zhao et al., 2016) and, thus, the positive ion mode was not further analyzed in providing structural insights in the current

305   study. The negative chromatogram peaks with RT at 11.85 min (N-145), 16.13 min (N-159), and 20.41 min (N-173) were significant peaks for cyclooctene SOA (Fig. 3b), and they were assigned neutral formulas of $C_6H_{10}O_4$, $C_7H_{12}O_4$, and $C_8H_{14}O_4$, respectively. As shown in Fig. 4, MS/MS spectra of monomer $C_6H_{10}O_4$, $C_7H_{12}O_4$, and $C_8H_{14}O_4$ were similar. Taking $C_8H_{14}O_4$ as example (Fig. 4c), its fragmentation mass spectrum was

310   characterized by a loss of 44 Da (CO_2), suggesting the presence of carboxyl group. The neutral loss of 18 Da (H_2O) upon fragmentation of the parent ion ($C_8H_{13}O_4^-$, *m/z* =

173.08209) led to the production of an ion with m/z 155.07143. The loss of H_2O is an unspecific fragmentation mechanism, which is likely originated from a carboxyl or hydroxyl group (Noziere et al., 2015). The fragment ion (m/z = 111.08166) representing

315 the simultaneous neutral losses of CO_2 and H_2O was also formed. MS/MS spectra can be resulted from multiple isomeric structures in many cases (Wang et al., 2019). Yasmeen et al. (2011) showed the detailed fragmentation spectrum for the dicarboxylic acid standard (azelaic acid) and indicated that deprotonated azelaic acid also showed losses of H_2O, CO_2, and CO_2 + H_2O. In addition, Noziere et al. (2015) showed that the

320 neutral losses of CO_2 and H_2O indicates two carboxyl groups. Thus, monomer $C_8H_{14}O_4$ was tentatively assigned to suberic acid and the corresponding fragmentation pathways for $C_8H_{13}O_4^-$ is proposed in Fig. S4. The fragment ions originated from losses of H_2O, CO_2, and CO_2 + H_2O were also observed in MS/MS spectra of $C_6H_{10}O_4$ and $C_7H_{12}O_4$, indicative of adipic acid and pimelic acid, respectively. Carboxylic acids have also been

325 observed in SOA produced from previous alkene ozonolysis (Hamilton et al., 2006; Kenseth et al., 2020; Mackenzie-Rae et al., 2018; Zhang et al., 2015). Carboxylic acids represent a significant class of aerosol components, and they play a significant role in particle chemistry by their influences on particle acidity and through direct involvement in certain heterogeneous reactions to produce low volatile species (Millet et al., 2015).

330 More experiments using available authentic standards are necessary to better understand their structures, sources, and formation mechanism. Other prominent monomer peaks at RTs 8.30 min (N-175) and 14.18 min (N-189) corresponded to compounds with neutral formula, namely $C_7H_{12}O_5$ and $C_8H_{14}O_5$. The losses of H_2O, CO, and CO_2 in MS/MS spectrum of $C_7H_{12}O_5$ indicated hydroxyl, terminal carbonyl,

335 and carboxyl group, respectively (Mackenzie-Rae et al., 2018; Riva et al., 2016a), and $C_7H_{12}O_5$ was identified as hydroxy-containing oxoheptanoic acid (Fig. S5a and S5c). Monomer $C_8H_{14}O_5$ only showed losses of H_2O and CO (Fig. S5b), and it is difficult to determine the specific type and positioning of oxygen-containing functionalities within $C_8H_{14}O_5$ with 5 oxygen atoms based on its MS/MS spectrum.
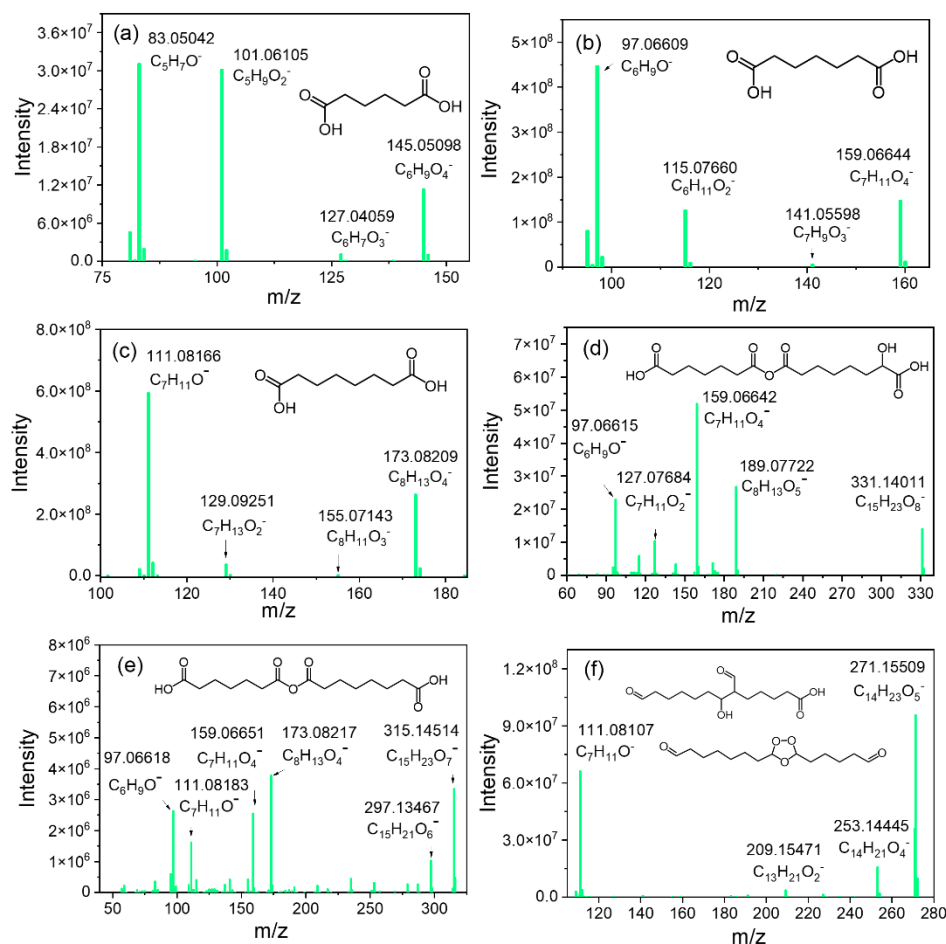
Figure 4. MS/MS spectra of major monomers and dimers. Monomers: (a) $C_6H_{10}O_4$, (b) $C_7H_{12}O_4$, and (c) $C_8H_{14}O_4$. Dimers: (d) $C_{15}H_{24}O_8$, (e) $C_{15}H_{24}O_7$, and (f) $C_{14}H_{24}O_5$.

The labeled dimer peaks in negative ion mode corresponded to $[M-H]^-$ ion masses of 271, 285, and 331 (Fig. 3b), which were assigned neutral formulas of $C_{14}H_{24}O_5$, $C_{15}H_{26}O_5$, and $C_{15}H_{24}O_8$, respectively. The number of fragment ions of dimers are generally limited, and determining the exact structure of dimers is less certain compared to monomers (Witkowski and Gierczak, 2017). Therefore, only a decrease in molecular structure possibilities is provided. For dimer $C_{15}H_{24}O_8$, fragment ions m/z 159.06642 ($C_7H_{11}O_4^-$) and m/z 189.07722 ($C_8H_{13}O_5^-$) were detected in its MS/MS spectrum (Fig. 4d). When dimers are subjected to CID, fragment ions corresponding to their building blocks are commonly observed (Witkowski and Gierczak, 2017; Hall and Johnston, 2012). Based on this rule, it could be concluded that dimer $C_{15}H_{24}O_8$ was an association product of $C_7H_{12}O_4$ and $C_8H_{14}O_5$. Similarly, for dimer $C_{15}H_{24}O_7$, there were two

significant product ions of $C_{15}H_{23}O_7^-$ with accurate masses of m/z 159.06651 ($C_7H_{11}O_4^-$)

355   and 173.08217 ($C_8H_{13}O_4^-$) (Fig. 4e). Furthermore, fragment ions corresponding to

secondary loss of $CO_2 + H_2O$ from product ions $C_7H_{11}O_4^-$ and $C_8H_{13}O_4^-$ were also

observed. The fragmentation spectrum of $C_{15}H_{24}O_7$ was similar to the MS/MS spectra

of $C_7H_{12}O_4$ and $C_8H_{14}O_4$ (Fig. 4b and 4c), suggesting again that $C_7H_{12}O_4$ and $C_8H_{14}O_4$

may be the building blocks of $C_{15}H_{24}O_7$. Acid-catalyzed heterogeneous processes can

360   result in the formation of high-molecular-weight dimers in both biogenic and

anthropogenic systems (Barsanti et al., 2017). Carboxylic acid monomers formed could

be important sources of particle acidity in the absence of SO_2. Dimers $C_{15}H_{24}O_7$ and

$C_{15}H_{24}O_8$ may be produced by heterogeneous reactions involving the loss of a water

molecule, and the linkage between building blocks is an acid anhydride (Fig. S6)

365   (Hamilton et al., 2006). Another abundant dimer peak (N-271) in negative

chromatogram was identified as $C_{14}H_{23}O_5^-$ with mass accuracy of -0.02492 ppm.

$C_{14}H_{23}O_5^-$ could dissociate to the product ions of $C_{14}H_{21}O_4^-$, $C_{13}H_{21}O_2^-$, and $C_7H_{11}O^-$.

(Fig. 4f). Both secondary ozonide and aldol structures shown in Fig. 4f could match the

assigned elemental formula of $C_{14}H_{24}O_5$. However, the neutral losses of H_2O and CO_2

370   were not easily produced by secondary ozonide, but more likely for the aldol structure

(Hall and Johnston, 2012). Aldol condensation products were also one of the most

commonly observed species in previous ozonolysis of alkenes (Zhao et al., 2016;

Kenseth et al., 2018; Kristensen et al., 2016). Therefore, $C_{14}H_{24}O_5$ shown in Fig. 4f is

likely an aldol condensation product.

375   To examine the overall composition of particles, average mass spectra (Fig. S7)

corresponding to the chromatogram where particle components eluted were also

analyzed. Figure 5 summarizes the oxidation products observed in particles mapped in

O-KMD and van Krevelen plot. The molecular formulas of identified oxidation

products could be largely classified into homologous series of monomers and dimers

380   (Fig. 5a and 5b). The elemental composition distribution of products measured in

positive and negative ion modes was similar, with most monomers and dimers having

O/C ratios ranging from 0.2 to 0.8, and H/C ratios ranging from 1.2 to 1.8 (Fig. 5c). Lines with slopes of 0, -0.5, -1, and -2 in Fig. 5c can be used to illustrate the addition of hydroxyl/peroxide, carboxylic acid (with fragmentation), carboxylic acid (without

385   fragmentation), and carbonyl groups to a saturated carbon chain, respectively (Heald et al., 2010). As shown in Fig. 5c, cyclooctene SOA occupied a relatively wide range in the van Krevelen diagram, and the large number of points scattered in the space between lines with slopes of -0.5 and -2. This behavior is consistent with the importance of high abundance carboxylic acids in the above analysis.

390   **3.3 SO$_2$ effects on aerosol chemical composition**

To further get detailed mechanisms about SO$_2$ effects and determine whether heterogeneous processes occurred, aerosol samples were analyzed using ATR-FTIR and LC/ESI-MS. Both IR and MS analysis of particles revealed changes in aerosol chemical composition induced by SO$_2$ addition.

395   **3.3.1 Characteristics of functional group in aerosol-phase products**

Figure 2 shows ATR-FTIR spectra of aerosol particles. Hydroxy (3600–3200 cm^{-1}), alkyl (2935 and 2864 cm^{-1}), and carbonyl (1702 cm^{-1}) were identified in particles collected from the cyclooctene/O$_3$ system (Table S1). These particles also had a broad absorption across the 1500–800 cm^{-1} region, which may arise from C–H deformation

400   in 1480–1350 cm^{-1}, C–C stretching in 1250–1120 cm^{-1}, and C–O stretching in different regions for various oxygenated species (Hung et al., 2013). Three additional absorption bands at 1413, 1095, and 617 cm^{-1} were observed in ATR-FTIR spectra of particles formed with the introduction of SO$_2$ (Tammer, 2004; Lal et al., 2012). Absorption bands at 1413 and 1095 cm^{-1} may be associated with the asymmetric and symmetric stretching

405   of -SO$_2$- while inorganic sulfates could give rise to strong absorption at 617 cm^{-1}. The presence of absorption band of sulfur-containing groups suggests that SO$_2$ addition can result in the production of sulfur-containing compounds.
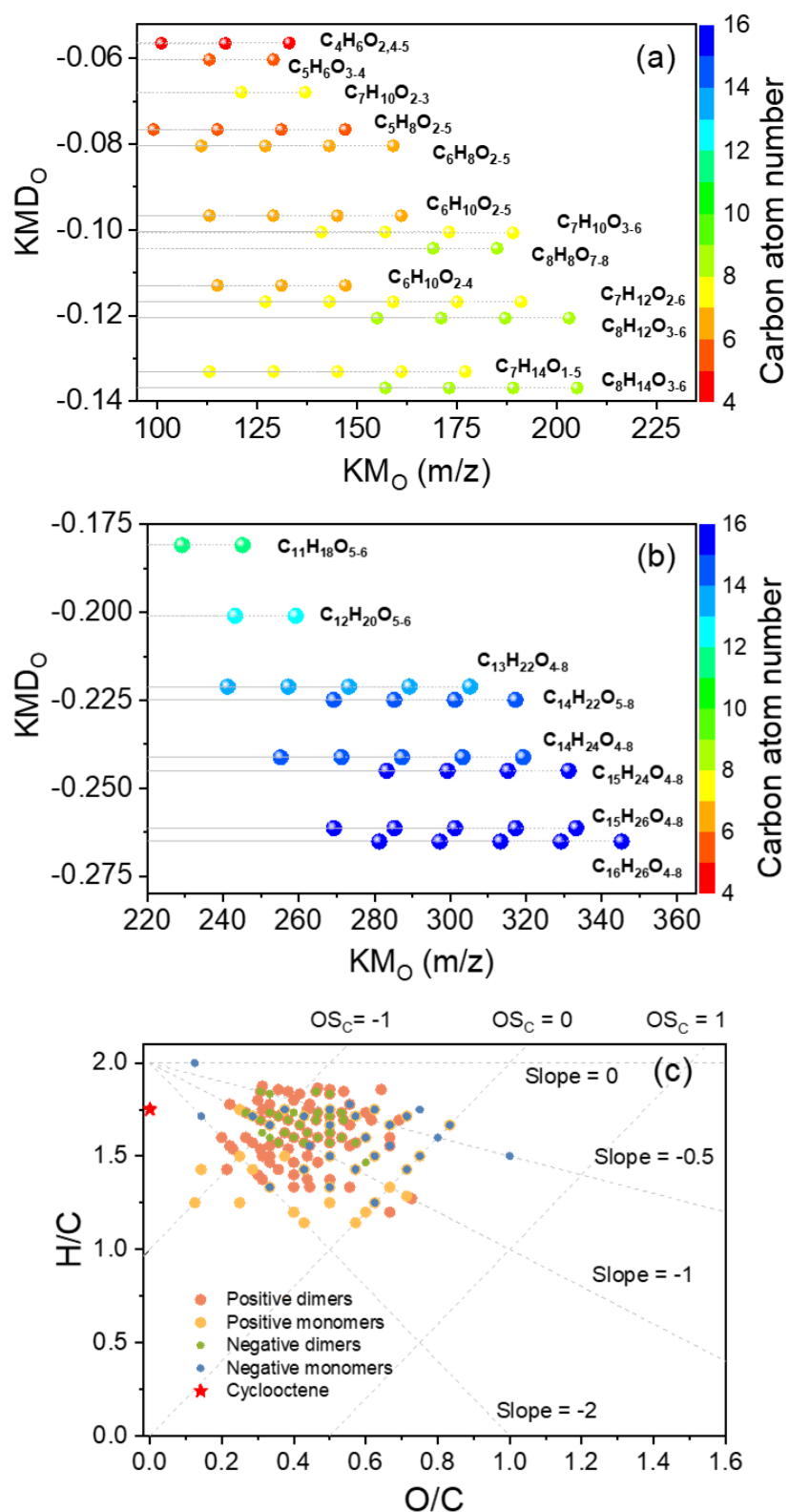
Figure 5. Oxidation products observed in particles produced from the ozonolysis of cyclooctene in the absence of SO_2. Oxygen (O)-Kendrick mass defect plots of (a) monomers and (b) dimers. (c) Van Krevelen diagram.

3.3.2 Organosulfate formation in the presence of SO_2

In addition to CHO compounds, products with $C_cH_hO_oS_s$ elemental formulas were identified in the presence of SO_2 (Fig. S8). OS could undergo highly efficient ionization to give deprotonated molecular ions in negative ion mode. Based on MS/MS analysis, unambiguous identification of OS can be achieved since OSs could give characteristic fragment ions at m/z 80 (SO_3^-), 81 (HSO_3^-), and/or 97 (HSO_4^-) in their MS/MS spectra (Figs. S9–S17). Accurate mass measurements of OSs as well as their retention times and DBE values are provided in Table S2. The proposed structure and fragmentation scheme of each OS and corresponding precursor are presented in Figs. S9–S17. For instance, OS-209 and OS-223 showed prominent product ions for losses of HSO_4^- and SO_3^- (Figs. S11–S12), confirming the organosulfate moiety. Neither a hydroxyl nor a carboxyl group fragment ion (i.e., $-H_2O$ or $-CO_2$) was observed in their MS/MS spectra. $C_6H_{10}O_3$ and $C_7H_{12}O_3$ were proposed as the precursor of OS-209 and OS-223, respectively. MS/MS spectra of $C_6H_{10}O_3$ and $C_7H_{12}O_3$ were characterized by loss of CO, indicating terminal carbonyl group (Figs. S11–S12). Considering structural features of OS precursor measurements as well as OS-209 and OS-223 all corresponding to DBE = 2, two terminal carbonyl groups could explain well the observed MS/MS spectra of OS-209 and OS-223. The organosulfate substituent was expected to attach to internal carbon atom. Although the carbonyl group is more readily observed in positive ion mode, ESI-MS is also highly sensitive to carbonyl compounds containing sulfate substituents and thereby gives intense $[M - H]^-$ ions in negative ion mode (Riva et al., 2016b).

Relatively high abundance of OS is helpful for the acquisition of MS/MS data, and therefore high abundance $[M - H]^-$ ions were chosen as representative candidates to clarify the precursors and formation pathways of OSs. Simplified chemical mechanism describing OS production from the ozonolysis of cyclooctene (C_8H_{14}) is proposed in Fig. 6. The ozonolysis of cyclooctene (C_8H_{14}) can be initiated by O_3 addition to the endocyclic double bond, forming an energy-rich primary ozonide (POZ). POZ can

decompose rapidly to an excited CI containing both a terminal carbonyl and carbonyl oxide group. The excited CI could lead to the formation of sCI, vinylhydroperoxide, and dioxirane, illustrating the multiplicity and the complexity of cyclooctene ozonolysis. SCI is mainly capable of involving in bimolecular reactions to form carboxylic acids and acid esters. Vinylhydroperoxide rapidly decomposes into an alkyl radical ($C_8H_{13}O_2\cdot$) and an $\cdot OH$. Molecular oxygen could be subsequently added to $C_8H_{13}O_2\cdot$ to produce an alkyl peroxy radical (RO$_2$, $C_8H_{13}O_4\cdot$). Dioxirane intermediate may also undergo decomposition and produce a $C_7H_{13}O_3\cdot$. $C_8H_{13}O_4\cdot$ and $C_7H_{13}O_3\cdot$ are considered as the starting point of the RO$_2\cdot$ and alkoxy radical (RO$\cdot$) chemistry, resulting in termination CHO compounds with hydroperoxy, carbonyl, or hydroxy groups (Fig. 6). Acid-catalyzed heterogenous reactions of CHO products have been evidenced to play a major role in OS formation in the atmosphere (Riva et al., 2016c; Riva et al., 2016b). Although acidic seed particles were not directly injected into the reactor during cyclooctene ozonolysis, SO$_2$-induced H_2SO_4 may create acidic conditions for the occurrence of heterogeneous reaction. In the case of CHO products with hydroxyl group, H_2SO_4 could protonate the hydroxyl group, leading to the formation of OS and water. The low RH ($\sim$ 20%) of ozonolysis was helpful for shifting the reaction equilibrium in favor of OS production.

Detailed information about the volatility of oxidation products is necessary to evaluate their potential to contribute to aerosol formation. As shown in Fig. 7a, the products could be categorized into intermediate volatility OCs (IVOCs), semi-volatile OCs (SVOCs), low-volatile OCs (LVOCs), and extremely low-volatile OCs (ELVOC) with C^o in the range of 300–3 $\times$ 10^6, 0.3–300, 3 $\times$ 10^{-4}–0.3, and < 3 $\times$ 10^{-4} μg m^{-3}, respectively (Donahue et al., 2011). The saturation mass concentration of OSs spanned more than 6 orders of magnitude (Fig. 7a), suggesting their inherent chemical complexity of them. A large number of OSs are SVOCs and LVOCs while their precursors are classified as IVOCs and SVOCs, indicating that the SO$_2$ presence facilitates the reduction of product volatility (Yang et al., 2020; Han et al., 2016).

Lower-volatile OSs generated from acid-catalyzed heterogenous reactions may build

470   particle mass at a faster rate compared to their higher-volatile precursors, and thereby

benefit the formation and growth of particles in the presence of SO_2.
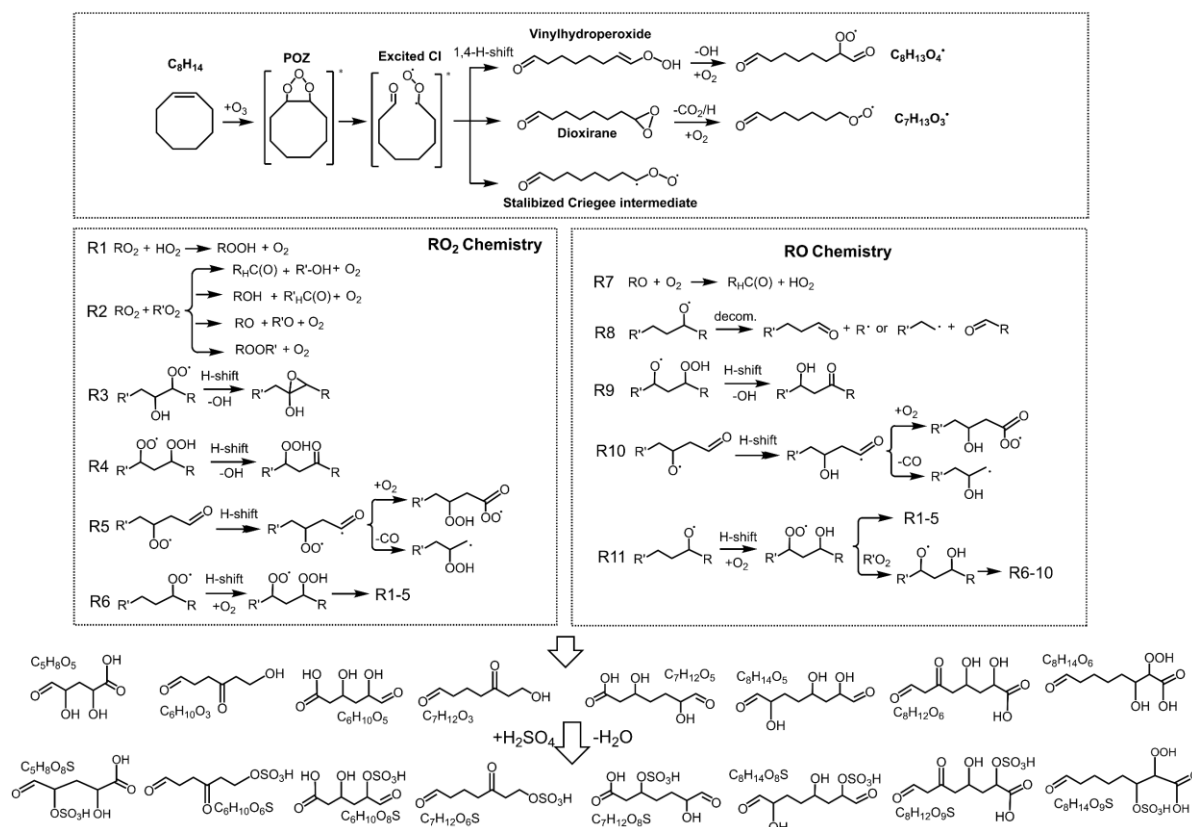
Figure 6. Simplified formation schemes for the selected organosulfates formed from

475   the ozonolysis of cyclooctene.

Figure 7b displays the DBE–carbon atom number space for organosulfur

compounds. There are some overlaps of organosulfur compounds detected in this work

with previous data from field observations (Wang et al., 2021b; Boris et al., 2016; Cai

480   et al., 2020). For example, Wang et al. (2021b) comprehensively analyzed OS in $PM_{2.5}$

filter samples collected in an urban site in Shanghai, China and observed the presence

of $C_6H_{10}O_6S$ (Fig. 7b, cyan cross). In the absence of chromatographic data such as

retention times, $C_6H_{10}O_6S$ was tentatively assigned to diesel vapor-derived OS. Alkenes

are important components of diesel and cyclooctene may be also responsible for

485 $C_6H_{10}O_6S$ formation in the atmosphere. The overlaps of organosulfur compounds indicate that the ozonolysis of cycloalkenes in the presence of SO_2 is likely an important source of organosulfur compounds in the ambient atmosphere. In addition, our work further suggests that the sources of OS cannot be determined only based on their elemental formula, and techniques that enable the identification of molecular structures

490 (e.g., MS/MS) are greatly beneficial in field studies. The identified molecular structures of OSs in this study are also helpful in the source apportionment in field studies.
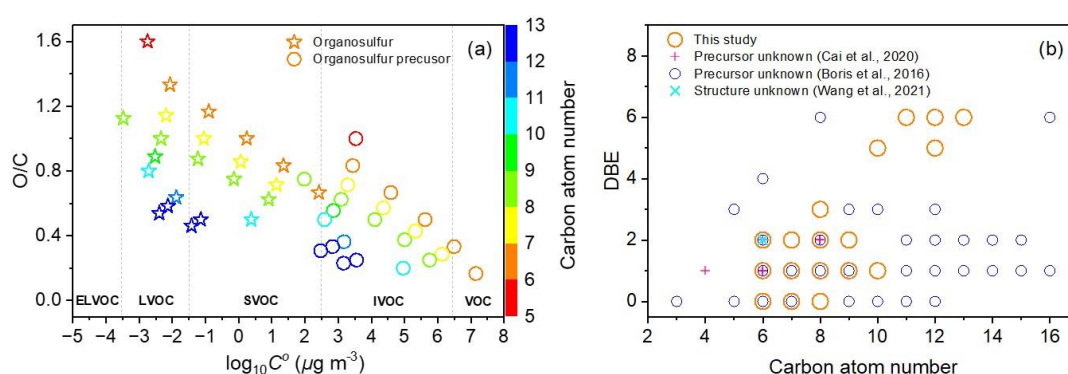
Figure 7. (a) Two dimensional volatility–oxidation space of the identified
495 organosulfurs and their precursors. (b) Carbon atom number distribution of organosulfurs observed in the current work and in the studies of Cai et al. (2020), Boris et al. (2016), and Wang et al. (2021b). Detailed formulae of these OSs can be found in Table S3. Organosulfurs from previous studies are of unknown origin or unknown structure.

500 **4 Conclusion**

We have explored O_3-initiated oxidation of cyclooctene in the absence and presence of SO_2, with a focus on the mechanism by which SO_2 impacts particle formation and composition. Cyclooctene can produce a large number of particles upon reacting with O_3. Higher SO_2 concentration led to higher particle number concentration
505 as a result of H_2SO_4 formation from the reactions of sCI with SO_2.

Cyclooctene SOA mainly consisted of carboxylic acids and corresponding dimers

with acid anhydride and aldol structures when SO_2 was not added. SO_2 addition can induce the changes in particle chemical composition through the formation of OSs. Some OSs, classified as compounds of unknown origin or unknow structure in previous field studies, were also observed in this work. The OSs found here are less volatile than their precursors, indicating the stronger ability of OS for particle formation. The formation of OSs can in part lead to the increase in particle volume concentrations in the presence of SO_2.

The results here suggest that SO_2 can influence aerosol particle formation and composition by producing sulfur-containing compounds (i.e., H_2SO_4 and OSs). Nevertheless, the observed number of OSs may be amplified by the high SO_2 concentration used in the present work. In order to determine the actual mass yields of OSs and better quantify SO_2 roles in particle formation, further experiments using ambient SO_2 levels and authentic standards are warranted.

Data availability.

Experimental data are available upon request to the corresponding author.

Supplement.

The supplement related to this article is available online at:

Author contribution.

ZY designed the experiments and carried them out. ZY performed data analysis with assistance from XL, NTT, KL, and LD. ZY prepared the paper with contributions from all co-authors. NTT, KL, and LD commented on the paper.

530 **Declaration.**

The authors declare that they have no conflict of interest.

Financial support.

This work was supported by National Natural Science Foundation of China (no. 22076099), Youth Innovation Program of Universities in Shandong Province (no. 535 2019KJD007), and Fundamental Research Fund of Shandong University (no. 2020QNQT012).

References

Apsokardu, M. J. and Johnston, M. V.: Nanoparticle growth by particle-phase chemistry, Atmos. Chem. Phys., 18, 1895-1907, 10.5194/acp-18-1895-2018, 2018.

Barsanti, K. C., Kroll, J. H., and Thornton, J. A.: Formation of Low-Volatility Organic Compounds in the Atmosphere: Recent Advancements and Insights, J Phys Chem Lett, 8, 1503-1511, 10.1021/acs.jpclett.6b02969, 2017.

Boris, A. J., Lee, T., Park, T., Choi, J., Seo, S. J., and Collett Jr, J. L.: Fog composition at Baengnyeong Island in the eastern Yellow Sea: detecting markers of aqueous atmospheric oxidations, Atmos. Chem. Phys., 16, 437-453, 10.5194/acp-16-437-2016, 2016.

Boy, M., Mogensen, D., Smolander, S., Zhou, L., Nieminen, T., Paasonen, P., Plass-Dülmer, C., Sipilä, M., Petäjä, T., Mauldin, L., Berresheim, H., and Kulmala, M.: Oxidation of SO_2 by stabilized Criegee intermediate (sCI) radicals as a crucial source for atmospheric sulfuric acid concentrations, Atmos. Chem. Phys., 13, 3865-3879, 10.5194/acp-13-3865-2013, 2013.

Bruggemann, M., Xu, R., Tilgner, A., Kwong, K. C., Mutzel, A., Poon, H. Y., Otto, T., Schaefer, T., Poulain, L., Chan, M. N., and Herrmann, H.: Organosulfates in Ambient Aerosol: State of Knowledge and Future Research Directions on Formation, Abundance, Fate, and Importance, Environ. Sci. Technol., 54, 3767-3782, 10.1021/acs.est.9b06751, 2020.

Cai, D., Wang, X., Chen, J., and Li, X.: Molecular characterization of organosulfates in highly polluted atmosphere using ultra-high-resolution mass spectrometry, J. Geophys. Res.-Atmos., 125, e2019JD032253, 10.1029/2019jd032253, 2020.

Coury, C. and Dillner, A. M.: A method to quantify organic functional groups and inorganic compounds in ambient aerosols using attenuated total reflectance FTIR spectroscopy and multivariate chemometric techniques, Atmos. Environ., 42, 5923-5932, 10.1016/j.atmosenv.2008.03.026, 2008.

Deng, H., Lakey, P. S. J., Wang, Y., Li, P., Xu, J., Pang, H., Liu, J., Xu, X., Li, X., Wang, X., Zhang, Y., Shiraiwa, M., and Gligorovski, S.: Daytime SO_2 chemistry on ubiquitous urban surfaces as a source of organic sulfur compounds in ambient air, Sci. Adv., 8, eabq6830, doi:10.1126/sciadv.abq6830, 2022.

Deng, Y., Inomata, S., Sato, K., Ramasamy, S., Morino, Y., Enami, S., and Tanimoto, H.: Temperature and acidity dependence of secondary organic aerosol formation from α-pinene ozonolysis with a compact chamber system, Atmos. Chem. Phys., 21, 5983-6003, 10.5194/acp-21-5983-2021, 2021.

Donahue, N. M., Epstein, S. A., Pandis, S. N., and Robinson, A. L.: A two-dimensional volatility basis set: 1. organic-aerosol mixing thermodynamics, Atmos. Chem. Phys., 11, 3303-3318, 10.5194/acp-11-3303-2011, 2011.

Fan, Y., Liu, C.-Q., Li, L., Ren, L., Ren, H., Zhang, Z., Li, Q., Wang, S., Hu, W., Deng, J., Wu, L., Zhong, S., Zhao, Y.,

Pavuluri, C. M., Li, X., Pan, X., Sun, Y., Wang, Z., Kawamura, K., Shi, Z., and Fu, P.: Large contributions of biogenic and anthropogenic sources to fine organic aerosols in Tianjin, North China, Atmos. Chem. Phys., 20, 117-137, 10.5194/acp-20-117-2020, 2020.

Gao, S., Keywood, M., Ng, N. L., Surratt, J., Varutbangkul, V., Bahreini, R., Flagan, R. C., and Seinfeld, J. H.: Low-molecular-weight and oligomeric components in secondary organic aerosol from the ozonolysis of cycloalkenes and alpha-pinene, J. Phys. Chem. A, 108, 10147-10164, 10.1021/jp047466e, 2004.

Hall, W. A. and Johnston, M. V.: Oligomer Formation Pathways in Secondary Organic Aerosol from MS and MS/MS Measurements with High Mass Accuracy and Resolving Power, Journal of the American Society for Mass Spectrometry, 23, 1097-1108, 10.1007/s13361-012-0362-6, 2012.

Hamilton, J. F., Lewis, A. C., Reynolds, J. C., Carpenter, L. J., and Lubben, A.: Investigating the composition of organic aerosol resulting from cyclohexene ozonolysis: low molecular weight and heterogeneous reaction products, Atmos. Chem. Phys., 6, 4973-4984, 10.5194/acp-6-4973-2006, 2006.

Han, Y., Stroud, C. A., Liggio, J., and Li, S.-M.: The effect of particle acidity on secondary organic aerosol formation from α-pinene photooxidation under atmospherically relevant conditions, Atmos. Chem. Phys., 16, 13929-13944, 10.5194/acp-16-13929-2016, 2016.

Hawkins, L. N., Russell, L. M., Covert, D. S., Quinn, P. K., and Bates, T. S.: Carboxylic acids, sulfates, and organosulfates in processed continental organic aerosol over the southeast Pacific Ocean during VOCALS-REx 2008, J. Geophys. Res., 115, D13201, 10.1029/2009jd013276, 2010.

He, X., Wang, Q., Huang, X. H. H., Huang, D. D., Zhou, M., Qiao, L., Zhu, S., Ma, Y.-g., Wang, H.-l., Li, L., Huang, C., Xu, W., Worsnop, D. R., Goldstein, A. H., and Yu, J. Z.: Hourly measurements of organic molecular markers in urban Shanghai, China: Observation of enhanced formation of secondary organic aerosol during particulate matter episodic periods, Atmos. Environ., 240, 117807, 10.1016/j.atmosenv.2020.117807, 2020.

Heald, C. L., Kroll, J. H., Jimenez, J. L., Docherty, K. S., DeCarlo, P. F., Aiken, A. C., Chen, Q., Martin, S. T., Farmer, D. K., and Artaxo, P.: A simplified description of the evolution of organic aerosol composition in the atmosphere, Geophys. Res. Lett., 37, L08803, 10.1029/2010gl042737, 2010.

Hettiyadura, A. P. S., Al-Naiema, I. M., Hughes, D. D., Fang, T., and Stone, E. A.: Organosulfates in Atlanta, Georgia: anthropogenic influences on biogenic secondary organic aerosol formation, Atmos. Chem. Phys., 19, 3191-3206, 10.5194/acp-19-3191-2019, 2019.

Huang, G., Liu, Y., Shao, M., Li, Y., Chen, Q., Zheng, Y., Wu, Z., Liu, Y., Wu, Y., Hu, M., Li, X., Lu, S., Wang, C., Liu, J., Zheng, M., and Zhu, T.: Potentially Important Contribution of Gas-Phase Oxidation of Naphthalene and Methylnaphthalene

to Secondary Organic Aerosol during Haze Events in Beijing, Environ. Sci. Technol., 53, 1235-1244, 10.1021/acs.est.8b04523, 2019.

Hung, H. M., Chen, Y. Q., and Martin, S. T.: Reactive aging of films of secondary organic material studied by infrared spectroscopy, J. Phys. Chem. A, 117, 108-116, 10.1021/jp309470z, 2013.

Kelly, J. M., Doherty, R. M., O'Connor, F. M., and Mann, G. W.: The impact of biogenic, anthropogenic, and biomass burning volatile organic compound emissions on regional and seasonal variations in secondary organic aerosol, Atmos. Chem. Phys., 18, 7393-7422, 10.5194/acp-18-7393-2018, 2018.

Kenseth, C. M., Hafeman, N. J., Huang, Y., Dalleska, N. F., Stoltz, B. M., and Seinfeld, J. H.: Synthesis of Carboxylic Acid and Dimer Ester Surrogates to Constrain the Abundance and Distribution of Molecular Products in alpha-Pinene and beta-Pinene Secondary Organic Aerosol, Environ. Sci. Technol., 54, 12829-12839, 10.1021/acs.est.0c01566, 2020.

Kenseth, C. M., Huang, Y., Zhao, R., Dalleska, N. F., Hethcox, J. C., Stoltz, B. M., and Seinfeld, J. H.: Synergistic O3 + OH oxidation pathway to extremely low-volatility dimers revealed in beta-pinene secondary organic aerosol, P. Natl. Acad. Sci. USA, 115, 8301-8306, 10.1073/pnas.1804671115, 2018.

Keywood, M. D., Varutbangkul, V., Bahreini, R., Flagan, R. C., and Seinfeld, J. H.: Secondary organic aerosol formation from the ozonolysis of cycloalkenes and related compounds, Environ. Sci. Technol., 38, 4157-4164, 10.1021/es035363o, 2004.

Kristensen, K., Watne, Å. K., Hammes, J., Lutz, A., Petäjä, T., Hallquist, M., Bilde, M., and Glasius, M.: High-Molecular Weight Dimer Esters Are Major Products in Aerosols from α-Pinene Ozonolysis and the Boreal Forest, Environ. Sci. Technol. Lett., 3, 280-285, 10.1021/acs.estlett.6b00152, 2016.

Kuang, B. Y., Lin, P., Hu, M., and Yu, J. Z.: Aerosol size distribution characteristics of organosulfates in the Pearl River Delta region, China, Atmos. Environ., 130, 23-35, 10.1016/j.atmosenv.2015.09.024, 2016.

Kundu, S., Fisseha, R., Putman, A. L., Rahn, T. A., and Mazzoleni, L. R.: Molecular formula composition of β-caryophyllene ozonolysis SOA formed in humid and dry conditions, Atmos. Environ., 154, 70-81, 10.1016/j.atmosenv.2016.12.031, 2017.

Lal, V., Khalizov, A. F., Lin, Y., Galvan, M. D., Connell, B. T., and Zhang, R.: Heterogeneous reactions of epoxides in acidic media, J. Phys. Chem. A, 116, 6078-6090, 10.1021/jp2112704, 2012.

Lehtipalo, K., Yan, C., Dada, L., Bianchi, F., Xiao, M., Wagner, R., Stolzenburg, D., Ahonen, L. R., Amorim, A., Baccarini, A., Bauer, P. S., Baumgartner, B., Bergen, A., Bernhammer, A. K., Breitenlechner, M., Brilke, S., Buchholz, A., Mazon, S. B., Chen, D. X., Chen, X. M., Dias, A., Dommen, J., Draper, D. C., Duplissy, J., Ehn, M., Finkenzeller, H., Fischer, L., Frege, C., Fuchs, C., Garmash, O., Gordon, H., Hakala, J., He, X. C., Heikkinen, L., Heinritzi, M., Helm, J. C., Hofbauer, V., Hoyle, C. R., Jokinen, T., Kangasluoma, J., Kerminen, V. M., Kim, C., Kirkby, J., Kontkanen, J., Kurten, A., Lawler, M. J., Mai, H. J.,

Mathot, S., Mauldin, R. L., Molteni, U., Nichman, L., Nie, W., Nieminen, T., Ojdanic, A., Onnela, A., Passananti, M., Petaja, T., Piel, F., Pospisilova, V., Quelever, L. L. J., Rissanen, M. P., Rose, C., Sarnela, N., Schallhart, S., Schuchmann, S., Sengupta, K., Simon, M., Sipila, M., Tauber, C., Tome, A., Trostl, J., Vaisanen, O., Vogel, A. L., Volkamer, R., Wagner, A. C., Wang, M. Y., Weitz, L., Wimmer, D., Ye, P. L., Ylisirnio, A., Zha, Q. Z., Carslaw, K. S., Curtius, J., Donahue, N. M., Flagan, R. C., Hansel, A., Riipinen, I., Virtanen, A., Winkler, P. M., Baltensperger, U., Kulmala, M., and Worsnop, D. R.: Multicomponent new particle formation from sulfuric acid, ammonia, and biogenic vapors, Sci. Adv., 4, eaau5363, 10.1126/sciadv.aau5363, 2018.

Li, Y., Pöschl, U., and Shiraiwa, M.: Molecular corridors and parameterizations of volatility in the chemical evolution of organic aerosols, Atmos. Chem. Phys., 16, 3327-3344, 10.5194/acp-16-3327-2016, 2016.

Liu, S., Jia, L., Xu, Y., Tsona, N. T., Ge, S., and Du, L.: Photooxidation of cyclohexene in the presence of SO_2: SOA yield and chemical composition, Atmos. Chem. Phys., 17, 13329-13343, 10.5194/acp-17-13329-2017, 2017.

Mackenzie-Rae, F. A., Wallis, H. J., Rickard, A. R., Pereira, K. L., Saunders, S. M., Wang, X., and Hamilton, J. F.: Ozonolysis of α-phellandrene – Part 2: Compositional analysis of secondary organic aerosol highlights the role of stabilised Criegee intermediates, Atmos. Chem. Phys., 18, 4673-4693, 10.5194/acp-18-4673-2018, 2018.

Millet, D. B., Baasandorj, M., Farmer, D. K., Thornton, J. A., Baumann, K., Brophy, P., Chaliyakunnel, S., de Gouw, J. A., Graus, M., Hu, L., Koss, A., Lee, B. H., Lopez-Hilfiker, F. D., Neuman, J. A., Paulot, F., Peischl, J., Pollack, I. B., Ryerson, T. B., Warneke, C., Williams, B. J., and Xu, J.: A large and ubiquitous source of atmospheric formic acid, Atmos. Chem. Phys., 15, 6283-6304, 10.5194/acp-15-6283-2015, 2015.

Nault, B. A., Jo, D. S., McDonald, B. C., Campuzano-Jost, P., Day, D. A., Hu, W., Schroder, J. C., Allan, J., Blake, D. R., Canagaratna, M. R., Coe, H., Coggon, M. M., DeCarlo, P. F., Diskin, G. S., Dunmore, R., Flocke, F., Fried, A., Gilman, J. B., Gkatzelis, G., Hamilton, J. F., Hanisco, T. F., Hayes, P. L., Henze, D. K., Hodzic, A., Hopkins, J., Hu, M., Huey, L. G., Jobson, B. T., Kuster, W. C., Lewis, A., Li, M., Liao, J., Nawaz, M. O., Pollack, I. B., Peischl, J., Rappenglück, B., Reeves, C. E., Richter, D., Roberts, J. M., Ryerson, T. B., Shao, M., Sommers, J. M., Walega, J., Warneke, C., Weibring, P., Wolfe, G. M., Young, D. E., Yuan, B., Zhang, Q., de Gouw, J. A., and Jimenez, J. L.: Secondary organic aerosols from anthropogenic volatile organic compounds contribute substantially to air pollution mortality, Atmos. Chem. Phys., 21, 11201-11224, 10.5194/acp-21-11201-2021, 2021.

Nie, W., Yan, C., Huang, D. D., Wang, Z., Liu, Y., Qiao, X., Guo, Y., Tian, L., Zheng, P., Xu, Z., Li, Y., Xu, Z., Qi, X., Sun, P., Wang, J., Zheng, F., Li, X., Yin, R., Dallenbach, K. R., Bianchi, F., Petäjä, T., Zhang, Y., Wang, M., Schervish, M., Wang, S., Qiao, L., Wang, Q., Zhou, M., Wang, H., Yu, C., Yao, D., Guo, H., Ye, P., Lee, S., Li, Y. J., Liu, Y., Chi, X., Kerminen, V.-M., Ehn, M., Donahue, N. M., Wang, T., Huang, C., Kulmala, M., Worsnop, D., Jiang, J., and Ding, A.: Secondary organic

aerosol formed by condensing anthropogenic vapours over China's megacities, Nature Geoscience, 15, 255-261, 10.1038/s41561-022-00922-5, 2022.

Noziere, B., Kalberer, M., Claeys, M., Allan, J., D'Anna, B., Decesari, S., Finessi, E., Glasius, M., Grgic, I., Hamilton, J. F., Hoffmann, T., Iinuma, Y., Jaoui, M., Kahnt, A., Kampf, C. J., Kourtchev, I., Maenhaut, W., Marsden, N., Saarikoski, S., Schnelle-Kreis, J., Surratt, J. D., Szidat, S., Szmigielski, R., and Wisthaler, A.: The molecular identification of organic compounds in the atmosphere: state of the art and challenges, Chem. Rev., 115, 3919-3983, 10.1021/cr5003485, 2015.

Qiu, X., Wang, S., Ying, Q., Duan, L., Xing, J., Cao, J., Wu, D., Li, X., Chengzhi, X., Yan, X., Liu, C., and Hao, J.: Importance of Wintertime Anthropogenic Glyoxal and Methylglyoxal Emissions in Beijing and Implications for Secondary Organic Aerosol Formation in Megacities, Environ. Sci. Technol., 54, 11809-11817, 10.1021/acs.est.0c02822, 2020.

Räty, M., Peräkylä, O., Riva, M., Quéléver, L., Garmash, O., Rissanen, M., and Ehn, M.: Measurement report: Effects of NOx and seed aerosol on highly oxygenated organic molecules (HOMs) from cyclohexene ozonolysis, Atmos. Chem. Phys., 21, 7357-7372, 10.5194/acp-21-7357-2021, 2021.

Rissanen, M. P.: NO2 Suppression of Autoxidation-Inhibition of Gas-Phase Highly Oxidized Dimer Product Formation, ACS Earth Space Chem., 2, 1211-1219, 10.1021/acsearthspacechem.8b00123, 2018.

Riva, M., Budisulistiorini, S. H., Zhang, Z., Gold, A., and Surratt, J. D.: Chemical characterization of secondary organic aerosol constituents from isoprene ozonolysis in the presence of acidic aerosol, Atmos. Environ., 130, 5-13, 10.1016/j.atmosenv.2015.06.027, 2016a.

Riva, M., Barbosa, T. D. S., Lin, Y.-H., Stone, E. A., Gold, A., and Surratt, J. D.: Chemical characterization of organosulfates in secondary organic aerosol derived from the photooxidation of alkanes, Atmos. Chem. Phys., 16, 11001-11018, 10.5194/acp-16-11001-2016, 2016b.

Riva, M., Budisulistiorini, S. H., Zhang, Z., Gold, A., Thornton, J. A., Turpin, B. J., and Surratt, J. D.: Multiphase reactivity of gaseous hydroperoxide oligomers produced from isoprene ozonolysis in the presence of acidified aerosols, Atmos. Environ., 152, 314-322, 10.1016/j.atmosenv.2016.12.040, 2017.

Riva, M., Budisulistiorini, S. H., Chen, Y., Zhang, Z., D'Ambro, E. L., Zhang, X., Gold, A., Turpin, B. J., Thornton, J. A., Canagaratna, M. R., and Surratt, J. D.: Chemical Characterization of Secondary Organic Aerosol from Oxidation of Isoprene Hydroxyhydroperoxides, Environ. Sci. Technol., 50, 9889-9899, 10.1021/acs.est.6b02511, 2016c.

Stangl, C. M., Krasnomowitz, J. M., Apsokardu, M. J., Tiszenkel, L., Ouyang, Q., Lee, S., and Johnston, M. V.: Sulfur dioxide modifies aerosol particle formation and growth by ozonolysis of monoterpenes and isoprene, J. Geophys. Res.-Atmos., 124, 4800-4811, 2019.

Stirnweis, L., Marcolli, C., Dommen, J., Barmet, P., Frege, C., Platt, S. M., Bruns, E. A., Krapf, M., Slowik, J. G., Wolf,

R., Prévôt, A. S. H., Baltensperger, U., and El-Haddad, I.: Assessing the influence of NOx concentrations and relative humidity on secondary organic aerosol yields from α-pinene photo-oxidation through smog chamber experiments and modelling calculations, Atmos. Chem. Phys., 17, 5035-5061, 10.5194/acp-17-5035-2017, 2017.

Tammer, M.: G. Sokrates: Infrared and Raman characteristic group frequencies: tables and charts, Colloid and Polymer Science, 283, 235-235, 10.1007/s00396-004-1164-6, 2004.

Tilgner, A., Schaefer, T., Alexander, B., Barth, M., Collett Jr, J. L., Fahey, K. M., Nenes, A., Pye, H. O. T., Herrmann, H., and McNeill, V. F.: Acidity and the multiphase chemistry of atmospheric aqueous particles and clouds, Atmos. Chem. Phys., 21, 13483-13536, 10.5194/acp-21-13483-2021, 2021.

Wang, S., Liu, T., Jang, J., Abbatt, J. P. D., and Chan, A. W. H.: Heterogeneous interactions between SO2 and organic peroxides in submicron aerosol, Atmos. Chem. Phys., 21, 6647-6661, 10.5194/acp-21-6647-2021, 2021a.

Wang, X. K., Rossignol, S., Ma, Y., Yao, L., Wang, M. Y., Chen, J. M., George, C., and Wang, L.: Molecular characterization of atmospheric particulate organosulfates in three megacities at the middle and lower reaches of the Yangtze River, Atmos. Chem. Phys., 16, 2285-2298, 10.5194/acp-16-2285-2016, 2016.

Wang, Y., Ma, Y., Li, X., Kuang, B. Y., Huang, C., Tong, R., and Yu, J. Z.: Monoterpene and Sesquiterpene alpha-Hydroxy Organosulfates: Synthesis, MS/MS Characteristics, and Ambient Presence, Environ. Sci. Technol., 53, 12278-12290, 10.1021/acs.est.9b04703, 2019.

Wang, Y., Zhao, Y., Wang, Y., Yu, J.-Z., Shao, J., Liu, P., Zhu, W., Cheng, Z., Li, Z., Yan, N., and Xiao, H.: Organosulfates in atmospheric aerosols in Shanghai, China: seasonal and interannual variability, origin, and formation mechanisms, Atmos. Chem. Phys., 21, 2959-2980, 10.5194/acp-21-2959-2021, 2021b.

Wang, Y., Hu, M., Guo, S., Wang, Y., Zheng, J., Yang, Y., Zhu, W., Tang, R., Li, X., Liu, Y., Le Breton, M., Du, Z., Shang, D., Wu, Y., Wu, Z., Song, Y., Lou, S., Hallquist, M., and Yu, J.: The secondary formation of organosulfates under interactions between biogenic emissions and anthropogenic pollutants in summer in Beijing, Atmos. Chem. Phys., 18, 10693-10713, 10.5194/acp-18-10693-2018, 2018.

Witkowski, B. and Gierczak, T.: Characterization of the limonene oxidation products with liquid chromatography coupled to the tandem mass spectrometry, Atmos. Environ., 154, 297-307, 10.1016/j.atmosenv.2017.02.005, 2017.

Wyche, K. P., Monks, P. S., Ellis, A. M., Cordell, R. L., Parker, A. E., Whyte, C., Metzger, A., Dommen, J., Duplissy, J., Prevot, A. S. H., Baltensperger, U., Rickard, A. R., and Wulfert, F.: Gas phase precursors to anthropogenic secondary organic aerosol: detailed observations of 1,3,5-trimethylbenzene photooxidation, Atmos. Chem. Phys., 9, 635-665, 10.5194/acp-9-635-2009, 2009.

Yang, Z., Tsona, N. T., George, C., and Du, L.: Nitrogen-Containing Compounds Enhance Light Absorption of Aromatic-

Derived Brown Carbon, Environ. Sci. Technol., 56, 4005-4016, 10.1021/acs.est.1c08794, 2022.

Yang, Z., Xu, L., Tsona, N. T., Li, J., Luo, X., and Du, L.: SO_2 and NH_3 emissions enhance organosulfur compounds and fine particle formation from the photooxidation of a typical aromatic hydrocarbon, Atmos. Chem. Phys., 21, 7963-7981, 10.5194/acp-21-7963-2021, 2021.

Yang, Z., Tsona, N. T., Li, J., Wang, S., Xu, L., You, B., and Du, L.: Effects of NO_x and SO_2 on the secondary organic aerosol formation from the photooxidation of 1,3,5-trimethylbenzene: A new source of organosulfates, Environ. Pollut., 264, 114742, 10.1016/j.envpol.2020.114742, 2020.

Yao, L., Garmash, O., Bianchi, F., Zheng, J., Yan, C., Kontkanen, J., Junninen, H., Mazon, S. B., Ehn, M., Paasonen, P., Sipila, M., Wang, M., Wang, X., Xiao, S., Chen, H., Lu, Y., Zhang, B., Wang, D., Fu, Q., Geng, F., Li, L., Wang, H., Qiao, L., Yang, X., Chen, J., Kerminen, V.-M., Petaja, T., Worsnop, D. R., Kulmala, M., and Wang, L.: Atmospheric new particle formation from sulfuric acid and amines in a Chinese megacity, Science, 361, 278-281, 10.1126/science.aao4839, 2018.

Yasmeen, F., Szmigielski, R., Vermeylen, R., Gomez-Gonzalez, Y., Surratt, J. D., Chan, A. W., Seinfeld, J. H., Maenhaut, W., and Claeys, M.: Mass spectrometric characterization of isomeric terpenoic acids from the oxidation of alpha-pinene, beta-pinene, d-limonene, and Delta3-carene in fine forest aerosol, J Mass Spectrom, 46, 425-442, 10.1002/jms.1911, 2011.

Ye, J., Abbatt, J. P. D., and Chan, A. W. H.: Novel pathway of SO_2 oxidation in the atmosphere: reactions with monoterpene ozonolysis intermediates and secondary organic aerosol, Atmos. Chem. Phys., 18, 5549-5565, 10.5194/acp-18-5549-2018, 2018.

Zhang, X., McVay, R. C., Huang, D. D., Dalleska, N. F., Aumont, B., Flagan, R. C., and Seinfeld, J. H.: Formation and evolution of molecular products in alpha-pinene secondary organic aerosol, P. Natl Acad. Sci. U. S. A, 112, 14168-14173, 10.1073/pnas.1517742112, 2015.

Zhao, Y., Wingen, L. M., Perraud, V., and Finlayson-Pitts, B. J.: Phase, composition, and growth mechanism for secondary organic aerosol from the ozonolysis of alpha-cedrene, Atmos. Chem. Phys., 16, 3245-3264, 10.5194/acp-16-3245-2016, 2016.

Zhu, J., Penner, J. E., Lin, G., Zhou, C., Xu, L., and Zhuang, B.: Mechanism of SOA formation determines magnitude of radiative effects, P. Natl. Acad. Sci. USA, 114, 12685-12690, 10.1073/pnas.1712273114, 2017.